Encapsulated three-dimensional bioprinted structure seeded with urothelial cells: a new construction technique for tissue-engineered urinary tract patch

Yi-Peng Jin[1], Chong Shi[2], Yuan-Yi Wu[3], Ji-Lei Sun[3], Jiang-Ping Gao[4], Yong Yang[3]

[1]Department of Urology, Sixth Medical Center of Chinese People's Liberation Army General Hospital, Beijing 100048, China;
[2]The First Center of Department of Hepatobiliary Surgery, Fifth Medical Center of Chinese People's Liberation Army General Hospital, Beijing 100039, China;
[3]Department of Urology, Fourth Medical Center of Chinese People's Liberation Army General Hospital, Beijing 100048, China;
[4]Department of Urology, First Medical Center of Chinese People's Liberation Army General Hospital, Beijing 100853, China.

Abstract

Background: Traditional tissue engineering methods to fabricate urinary tract patch have some drawbacks such as compromised cell viability and uneven cell distribution within scaffold. In this study, we combined three-dimensional (3D) bioprinting and tissue engineering method to form a tissue-engineered urinary tract patch, which could be employed for the application on Beagles urinary tract defect mode to verify its effectiveness on urinary tract reconstruction.

Methods: Human adipose-derived stem cells (hADSCs) were dropped into smooth muscle differentiation medium to generate induced microtissues (ID-MTs), flow cytometry was utilized to detect the positive percentage for CD44, CD105, CD45, and CD34 of hADSCs. Expression of vascular endothelial growth factor A (VEGFA) and tumor necrosis factor-stimulated gene-6 (TSG-6) in hADSCs and MTs were identified by Western blotting. Then the ID-MTs were employed for 3D bioprinting. The bioprinted structure was encapsulated by transplantation into the subcutaneous tissue of nude mice for 1 week. After retrieval of the encapsulated structure, hematoxylin and eosin and Masson's trichrome staining were performed to demonstrate the morphology and reveal collagen and smooth muscle fibers, integral optical density (IOD) and area of interest were calculated for further semi-quantitative analysis. Immunofluorescent double staining of CD31 and α-smooth muscle actin (α-SMA) were used to reveal vascularization of the encapsulated structure. Immunohistochemistry was performed to evaluate the expression of interleukin-2 (IL-2), α-SMA, and smoothelin of the MTs in the implanted structure. Afterward, the encapsulated structure was seeded with human urothelial cells. Immunofluorescent staining of cytokeratins AE1/AE3 was applied to inspect the morphology of seeded encapsulated structure.

Results: The semi-quantitative assay showed that the relative protein expression of VEGFA was 0.355 ± 0.038 in the hADSCs *vs.* 0.649 ± 0.150 in the MTs ($t = 3.291$, $P = 0.030$), while TSG-6 expression was 0.492 ± 0.092 in the hADSCs *vs.* 1.256 ± 0.401 in the MTs ($t = 3.216$, $P = 0.032$). The semi-quantitative analysis showed that the mean IOD of IL-2 in the MT group was 7.67 ± 1.26, while 12.6 ± 4.79 in the hADSCs group, but semi-quantitative analysis showed that there was no statistical significance in the difference between the two groups ($t = 1.724$, $P = 0.16$). The semi-quantitative analysis showed that IOD was 71.7 ± 14.2 in non-induced MTs (NI-MTs) *vs.* 35.7 ± 11.4 in ID-MTs for collagen fibers ($t = 3.428$, $P = 0.027$) and 12.8 ± 1.9 in NI-MTs *vs.* 30.6 ± 8.9 in ID-MTs for smooth muscle fibers ($t = 3.369$, $P = 0.028$); furthermore, the mean IOD was 0.0613 ± 0.0172 in ID-MTs *vs.* 0.0017 ± 0.0009 in NI-MTs for α-SMA ($t = 5.994$, $P = 0.027$), while 0.0355 ± 0.0128 in ID-MTs *vs.* 0.0035 ± 0.0022 in NI-MTs for smoothelin ($t = 4.268$, $P = 0.013$), which indicate that 3D bioprinted structure containing ID-MTs could mimic the smooth muscle layer of native urinary tract. After encapsulation of the urinary tract patch for additional cell adhesion, urothelial cells were seeded onto the encapsulated structures, and a monolayer urothelial cell was observed.

Conclusion: Through 3D bioprinting and tissue engineering methods, we provided a promising way to fabricate tissue-engineered urinary tract patch for further investigation.

Keywords: Human adipose-derived stem cells; Urinary tract patch; Microtissues; Tissue engineering; Three-dimensional bioprinting

Access this article online

Quick Response Code:

Website: www.cmj.org

DOI: 10.1097/CM9.0000000000000654

Yi-Peng Jin and Chong Shi contributed equally to the work.

Correspondence to: Prof. Yong Yang, Department of Urology, Fourth Medical Center of Chinese People's Liberation Army General Hospital, Beijing 100048, China
E-Mail: yongyang301@163.com

Chinese Medical Journal 2020;133(4)

Received: 23-09-2019 **Edited by:** Qiang Shi

Introduction

Urinary tract stricture caused by catheterization, trauma, or infection often requires surgical intervention such as urinary tract reconstruction. The lack of available autologous materials such as buccal mucosa and prepuce drives researchers to seek substitute biomaterials through tissue engineering. Over the past decades, urinary tract reconstruction using various natural or synthetic biomaterials has emerged to address the issue, through the use of various materials including small intestinal submucosa, bladder acellular matrix (BAM), polyglycolic acid, poly lactic-co-glycolic acid (PLGA), etc.[1-4] Although natural and synthetic biomaterials each have their own merits, their drawbacks should not be ignored in their application. For natural biomaterials, which are often sourced from animals, the possibility of disease transmission and heterogeneity in the physical configuration of these xenografts remains an unsolved problem. For synthetic biomaterials, the lack of molecular signals diminishes cell attachment onto these biomaterials and therefore compromises cell activity and proliferation. Last but not least, neither natural nor synthetic biomaterials can achieve spatial cell distribution within the materials, which could expose cells to the outer environment, thus handicapping their function.

The traditional tissue engineering approach for fabricating urinary tract patch mainly depends on the cell-scaffold strategy: using a mold to produce a porous biomaterial, manually seeding smooth muscle cells, and urothelial cells (UCs) onto the biomaterial and waiting for cell infiltration. The seeding duration often lasts 1 week,[5,6] meaning a sandwich coculture or triculture of multiple types of cells in the porous biomaterial might require 2 to 3 weeks,[7,8] which makes building "off the shelf" tissue-engineered urinary tract patch difficult for research and clinical applications. Three-dimensional (3D) bioprinting, newly emanated from traditional additive manufacturing, is being utilized to overcome the drawbacks mentioned above in tissue engineering. Compared to the classic cell-scaffold strategy, 3D bioprinting could be used to construct a scaffold containing cells in a single step using certain biomaterials. Furthermore, with the assistance of computer design, the shape of the bioprinted structure could attain diversity without the constraint of the molds employed in the conventional tissue engineering approach. Our previous study verified that microtissues (MTs) composed of human adipose-derived stem cells (hADSCs) could enhance smooth muscle differentiation and cell viability during micro-extrusion 3D bioprinting[9]; hence, a bioprinted structure incorporating ID-MTs might provide a substrate for producing a tissue-engineered urinary tract patch. Here, we implanted a bioprinted structure into nude mice subcutaneously for encapsulation, and 1 week after implantation, UCs were seeded onto these encapsulated structures. In this study, we combined 3D bioprinting and tissue engineering method to form a tissue-engineered urinary tract patch, which could be employed for the application on Beagles urinary tract defect mode to verify its effectiveness on urinary tract reconstruction in further investigation.

Methods

Ethical approval

This study was approved by the Clinical Ethics Committee of Fourth Medical Center of People's Liberation Army General Hospital, and wavier of patient consent was approved.

Culture of human adipose-derived stem cells

The hADSCs were purchased from Cyagen (passage 2, Lot. HUXMD-01001, USA). Briefly, the purchased hADSCs were recovered in a 37°C water bath and then transferred to a 10-mL centrifuge tube. Next, 5 mL of culture medium (α-minimum Eagle's medium [α-MEM] containing 100 U/mL of penicillin/streptomycin and 10% fetal bovine serum, all purchased from Corning, USA) was added to suspend the cells. The cell suspension was centrifuged at 1500 × *g* for 5 min, then the supernatant was discarded, and the precipitate was resuspended with culture medium and seeded onto 10-cm petri dishes. When the cells reached 80% to 90% confluence, they were passaged by 0.25% ethylenediaminetetraacetic (EDTA)-trypsin (Solarbio, China).

Flow cytometry of hADSCs

Flow cytometry was utilized to characterize the hADSCs. Cells at passage 3 were digested with 0.25% EDTA-trypsin and washed three times in phosphate buffer saline (PBS; Keygen, China) after centrifugation (1500 × *g* for 5 min). Afterward, 1×10^4 cells/tube were incubated in the dark at room temperature for 20 min with the following primary antibodies: CD44 (fluorescein isothiocyanate [FITC] conjugated), CD105 (allophycocyanin conjugated), CD45 (phycoerythrin [PE] conjugated), CD34 (PE conjugated) (all purchased from BD Bioscience, USA), and fluorescence line height-2 was set as blank. Then, the cells were washed again twice with PBS, centrifuged (1500 × *g* for 5 min) and resuspended in 200 μL of PBS. Finally, CD surface antigens were analyzed with a flow cytometer (BD FACSCalibur, USA).

Generation of hADSCs microtissues

Passages 3 to 5 of the hADSCs were employed to generate MTs. As we previously described, the hanging-drop method was utilized to form MTs consisting of hADSCs.[9] Briefly, 5×10^5 hADSCs were suspended in 1 mL of culture medium or smooth muscle inductive medium (SMIM; culture medium supplemented with 10 ng/mL of transforming growth factor-β1; Sigma-Aldrich, USA) to form MTs based on gravity-forced cell assembly. The MTs (10,000 cells in 20 μL) generated in the culture medium were defined as non-induced MTs (NI-MTs), while the MTs generated in SMIM were defined as ID-MTs. Both NI-MTs and ID-MTs were kept for 3 days in a hanging-drop array at 37°C in a humidified atmosphere of 5% CO_2.

Western blotting

Adhered hADSCs were maintained in the culture medium, and NI-MTs were subjected to Western blotting. Cells were washed with 4°C PBS (Keygen) thrice and then lysed in a radioimmunoprecipitation assay (ApplyGen

Technology, China) to obtain the total protein. The concentration of total protein was measured with a bicinchoninic acid protein quantitation assay (Keygen). Thirty micrograms of protein was then separated using 8% sodium dodecyl sulfate-polyacrylamide gel electrophoresis and transferred to polyvinylidene fluoride (Millipore, USA) membranes. The membranes were blocked with 5% non-fat dry milk (Cell Signaling Technology, USA) in tris-buffered saline Tween-20 (TBST; ApplyGen Technology) buffer for 2 h. Then, the membranes were incubated with primary antibodies at 4°C overnight. The primary antibodies were as follows: rabbit polyclonal tumor necrosis factor alpha-stimulated gene-6 (TSG-6, 1:1000, Lot. ab128266; Abcam, UK), rabbit polyclonal vascular endothelial growth factor A (VEGFA) (1:1000, Lot. ab46154; Abcam), and mouse polyclonal β-actin (1:1000, Lot. ab20272; Abcam) antibodies. Next, the membranes were washed with TBST for 10 min three times. Then, the membranes were incubated with horseradish peroxidase (HRP)-conjugated anti-rabbit and anti-mouse IgG secondary antibodies (1:5000; ZSGB-BIO, China) for 90 min at room temperature and then washed thrice with TBST. After adding enhanced chemiluminescence detection reagents (ApplyGen Technology), the membranes were visualized by scanning the immunostaining band (GE ImageQuant LAS4000, USA). The band intensity was analyzed with Image-Pro-plus 6.0 software (Media Cybernetics, Inc., Rockville, MD, USA). And the results were represented as histograms with GraphPad Prism 6 Software (GraphPad Software, Inc., La Jolla, CA, USA).

Three-dimensional bioprinting

A micro-extrusion 3D bioprinter (Regenovo 3D bioprinter, China) was employed to fabricate a 3D structure containing hADSCs/NI-MTs/ID-MTs as we previously described.[9] Briefly, each group was embedded into hydrogels using a 20-mL hyperthermia-dissolved solution of 0.2 g/mL of gelatin (Sigma-Aldrich) mixed evenly with a 10-mL solution including 0.04 g/mL of sodium alginates (Sigma-Aldrich) at 25°C. We utilized a syringe with an orifice diameter of 340 μm for constructing the 3D structure, and all used syringes, syringe-paired inner sealers, and nozzles were autoclaved before the bioprinting process. First, the bioprinting platform with a temporal-fixed 60 mm petri dish used as a substrate was rapidly cooled for 45 min to 4°C and underwent ultraviolet sterilization. Then, we fabricated the desired 3D structure by maintaining the bioink at a temperature of less than 8°C during extrusion from the syringe and placement. Last, each fresh structure was immediately sprinkled with 2 mL of sterile 10% calcium chloride at 4°C for 10 min to complete the cross-linking process and then immersed in culture medium (hADSCs and NI-MTs) or SMIM (ID-MTs) and cultured in the incubator at 37°C in a humidified atmosphere of 5% CO_2.

Subcutaneous implantation of the bioprinted 3D structure

To encapsulate the bioprinted structure, three different bioprinted structures containing hADSCs/NI-MTs/ID-MTs were implanted subcutaneously into BALB/C nude mice (Vital River Laboratory Animal Technology, China, this experiment was approved by the Animal Ethics Committee of Fourth Medical Center of People's Liberation Army General Hospital), with two pieces of the structure per animal (20 male nude mice and 20 female nude mice). Briefly, 10-week-old mice were anesthetized through intraperitoneal injection of barbital (40 mg/kg), and then the dorsal skin midline was incised and blunt dissected to separate dorsal pockets (two pockets per animal). The structures were implanted into these separated pockets, and the incisions were closed by continuous suture. After 7 days, these nude mice were executed, and the implanted structures were harvested.

Histologic and immunofluorescent staining assay of retrieved structures

Freshly bioprinted and implanted structures retrieved from nude mice were fixed in 4% buffered formalin for 24 h and embedded in paraffin. Then, these samples were processed for histologic and immunofluorescent staining in sections of 4 μm. For histologic analysis, hematoxylin and eosin (HE) staining was employed to inspect the construction of implanted structures, and Masson's trichrome staining was utilized to reveal smooth muscle and collagen fibers in the implanted structures. In this staining process, smooth muscle fibers were stained with red, and collagen fibers were stained with blue.

Vascularization of implanted structures was revealed by immunofluorescent double staining of CD31 and α-smooth muscle actin (α-SMA). Sections of implanted structures were permeabilized and blocked with 0.1% Triton X-100 and 5% goat serum (ZSGB-BIO) in PBS (Keygen) for 15 min at room temperature. Then, sections were incubated with primary antibodies (mouse anti-human CD31 [ab24590], 1:500, and rabbit anti-human α-SMA [ab5694; Abcam] 1:300) overnight at 4°C. Afterward, the sections were incubated with FITC-conjugated goat anti-rabbit IgG, and Cy3-conjugated goat anti-mouse IgG (1:1000; Abcam) for 60 min at room temperature and rinsed with PBS thrice. For nuclear staining, the sections were incubated with 4′,6-diamidino-2-phenylindole (Keygen) for 15 min. Last, the sections were photographed and recorded using a LEICA DMI 4000B digital microscope camera system (Leica, Heidelberg, Germany).

To further investigate the phenotype of the NI-MTs and ID-MTs in the implanted structure, immunohistochemistry (IHC) was performed as follows. The sections were deparaffinized, and antigen retrieval was carried out by microwaving the sections for 6 min at 100°C in EDTA-antigen retrieval buffers (Servicebio, China). Then, the sections were washed with PBS thrice for 5 min and immersed in 3% hydrogen dioxide solution for 25 min. The sections were then washed with PBS three times again for 5 min and blocked by 3% bovine serum albumin (Solarbio) for 30 min at room temperature. Subsequently, the sections were incubated with primary antibodies (rabbit anti-human α-SMA, 1:300, Lot. ab5694; mouse anti-human smoothelin, 1:200, Lot. ab8969, all purchased from Abcam) at 4°C overnight, and then the sections were washed with PBS (Keygen) thrice and incubated with secondary antibodies (HRP-conjugated goat anti-rabbit and goat anti-mouse; DAKO, Denmark) for 50 min at room temperature. Then, the sections were washed with

PBS, and bound antibodies were detected using a 3,3′-diaminobenzidine detection kit (DAKO), followed by hematoxylin counterstaining for 3 min.

For Masson's trichrome staining and IHC staining of α-SMA and smoothelin, the integral optical density (IOD) and area of interest were calculated by Image-Pro-plus 6.0 software for further semi-quantitative analysis, and the results were represented as histograms with GraphPad Prism 6 Software.

Culture of ureteral urothelial cells

Human normal ureteral tissues came from patients undergoing radical nephrectomy. After collected, ureteral tissues were washed thrice with PBS at room temperature, and then split open with eye scissors, and washed with PBS three times again. Then, the mucosa was separated from the ureteral tissues by forcep and minced into 1 mm pieces. These pieces were gathered and placed onto a 6-cm petri dish and treated with 0.05% EDTA-trypsin (Solarbio) for 25 min at room temperature. The digestion carried out by trypsin was terminated with α-MEM containing 10% fetal bovine serum, and centrifuged for 5 min at 1590 × *g*. Then the suspension was discarded and the pellet was resuspended with 1.5 mL of keratinocyte serum-free media (KSFM; Gibco, USA) and added onto a 10-cm petri dish gently, then cultured in the incubator at 37°C in a humidified atmosphere of 5% CO_2. After 48 h of incubation, the outgrowth of cells from each piece of ureteral tissue can be observed, and 3 mL of additional KSFM was added to support cell growth. When UCs were 95% confluent, they were passaged by 0.05% EDTA-trypsin (Solarbio), and passages 3 to 6 of UCs were used to conduct further experiments.

Seeding of urothelial cells onto harvested structures and analysis of urothelial cells on the structures

UCs were seeded onto retrieved structures to construct tissue-engineered urinary tract patch. Briefly, UCs were detached from petri dishes and centrifuged. Then, the UCs were resuspended with KSFM, and the cell concentration was adjusted such that 1 mL of solution contained 5×10^5 cells. The retrieved structure was trimmed and transferred to 96-well plates. Then, 200 μL of the suspension of UCs was dropped onto the top of the retrieved structure, and the seeded structure was incubated at 37°C in a humidified atmosphere with 5% CO_2. To examine the seeded UCs on the implanted structure, immunofluorescent double staining of cytokeratins AE1/AE3 and α-SMA was conducted as aforementioned in the protocol for CD31 and α-SMA double staining, with the primary antibodies including mouse anti-human anti-pan cytokeratin antibody AE1/AE3 (1:300, ab961; Abcam), and rabbit anti-human α-SMA (1:300, ab5694; Abcam).

Statistical analysis

Statistical analyses were performed with SPSS 17.0 software (SPSS Inc., Chicago, IL, USA). All data are presented as the mean ± standard deviation. The comparison between groups was performed using *t* test, and a value of $P < 0.05$ was considered statistically significant.

Results

General inspection of hADSCs and MTs before and after 3D bioprinting

A large number of hADSCs were attained from the recovery of purchased hADSCs, and after 2 to 3 days of culture, the hADSCs presented the "hill-vally" morphology [Figure 1A]. Passage 4 of the hADSCs were harvested from the petri dish to generate MTs, and at day 3 after generation, the MTs were collected for use in 3D bioprinting [Figure 1B]. Correspondingly, passage 4 of the hADSCs was detached from the petri dish for 3D bioprinting as a control for microscopic observation. After the bioprinting process, both adhered hADSCs and MTs exhibited a shrunken diameter [Figure 1C and 1D], and the configuration of the adhered hADSCs was changed to a round shape, while the MTs largely maintained their morphology. The flow cytometry results showed that the hADSCs presented a strong positivity for CD44 and CD105, while no signal was detected for CD45 and CD34. The percentage of positive cells was 99.98%, 99.97%, 0.02%, and 0.04% [Figure 1].

Detection of VEGFA and TSG-6 expression in hADSCs and MTs by Western blotting assays

Non-induced adhered hADSCs and MTs were obtained for analysis of VEGFA and TSG-6 expression. Analysis showed that the expression of VEGFA and TSG-6 was much higher in MTs than in hADSCs. The semi-quantitative assay showed that the band intensity of VEGFA and TSG-6 in the MTs and hADSCs was 0.649 ± 0.150 *vs.* 0.355 ± 0.038, $t = 3.291$, $P = 0.030$, and 1.256 ± 0.401 *vs.* 0.492 ± 0.092, $t = 3.216$, $P = 0.032$, respectively [Figure 2]. These results were consistent with those of our previous study.[10]

Subcutaneous implantation and retrieval of 3D-bioprinted structures

Several 2 cm × 1 cm × 1 cm (length × width × height) structures were bioprinted for histologic analysis and subcutaneous implantation into nude mice. Figure 3A presents the gross inspection of the freshly bioprinted structure, and two pieces of the bioprinted structure were implanted into one animal subcutaneously [Figure 3B]. After *in vivo* maturation for 7 days, the implanted structures were extracted. After extraction, the structures had roughly held their configuration and were encapsulated, although some parts of the structures were fragmented [Figure 3C].

Histologic analysis and immunofluorescence

HE staining demonstrated the morphology of the implanted 3D structure [Figure 4]. After subcutaneous implantation for 7 days, both MTs and hADSCs were found to maintain their shape in the retrieved 3D structures.

Immunofluorescent double staining of CD31 and α-SMA revealed vascularization of the implanted structures

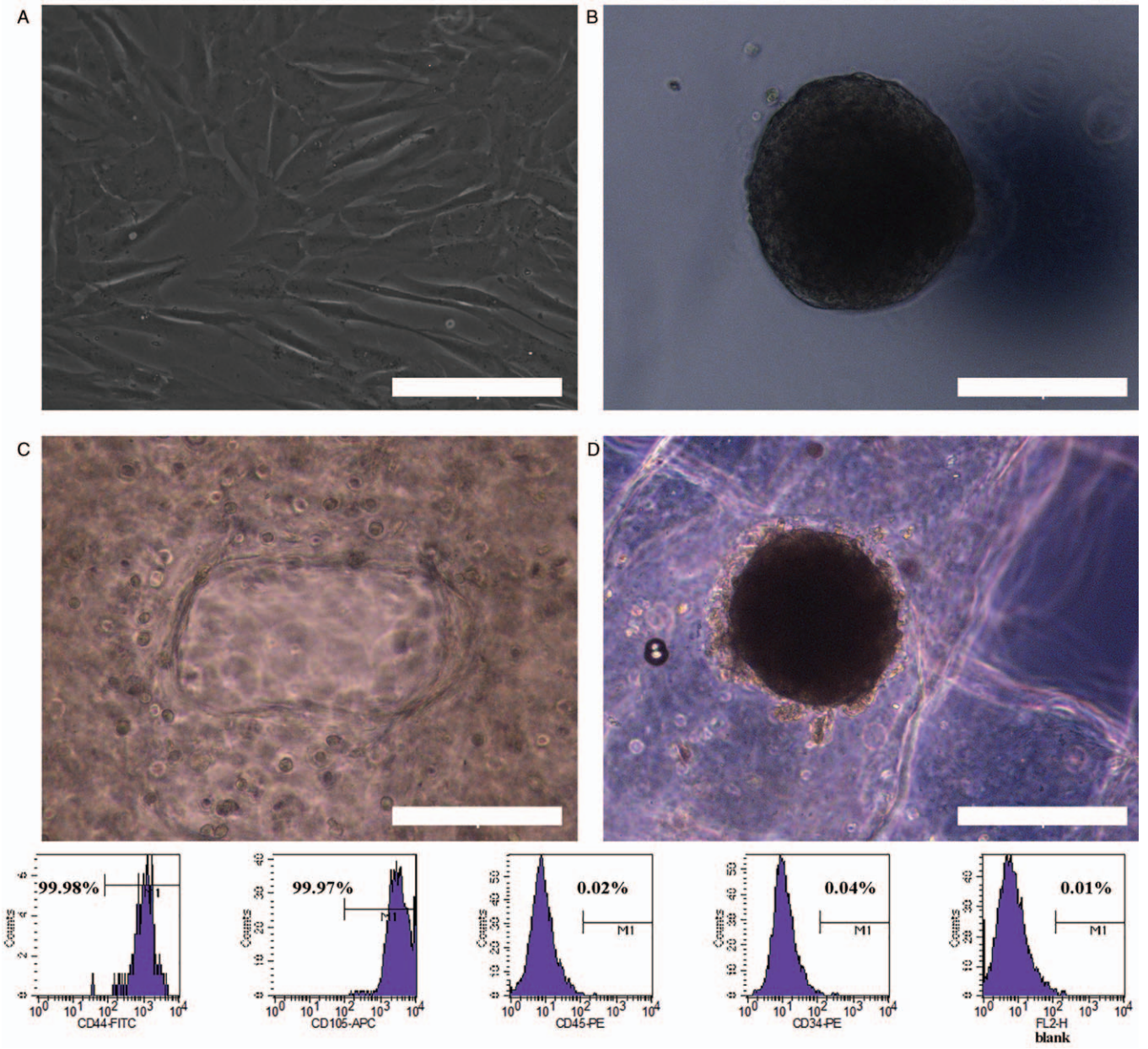

Figure 1: General inspection of hADSCs and MTs and identification of hADSCs. (A) Phase contrast microscopy showing the morphology of hADSCs. (B) Morphology of MTs. (C) Morphology of hADSCs after the bioprinting process. (D) Morphology of MTs after the bioprinting process. Scale bar = 200 μm. Bottom: Flow cytometry analysis of hADSCs surface phenotype. CD44 and CD105 were positive while CD45 and CD34 were negative. The percentage of positive cells is indicated in the figure. hADSCs: Human adipose-derived stem cells; MTs: Microtissues.

[Figure 5A]. As depicted, the bioprinted structure could form neo-vascular tissue (CD31 and α-SMA double-stained) in the MTs group, while only a little α-SMA was expressed and vascular morphology was hardly observed in the hADSCs group. The expression of interleukin (IL)-2 in the MTs group was lower than that in the hADSCs group [Figure 5B], but semi-quantitative analysis showed that there was no statistical significance in the difference between the two groups (MTs *vs.* hADSCs: 7.67 ± 1.26 *vs.* 12.6 ± 4.79, $t = 1.724$, $P = 0.16$).

Masson's trichrome staining revealed smooth muscle fibers and collagen fibers in the implanted structures [Figure 6]. As the test depicted, NI-MTs in the implanted structures could form several collagen fibers, but smooth muscle fibers were rare. Meanwhile, ID-MTs in the implanted structures generated collagen fibers and smooth muscle fibers at the same time. Semi-quantitative analysis showed that the mean IOD (mean IOD = IOD summation/area summation) was 71.7 ± 14.2 (NI-MTs) *vs.* 35.7 ± 11.4 (ID-MTs) for collagen fibers ($t = 3.428$, $P = 0.027$) and 12.8 ± 1.9 (NI-MTs) *vs.* 30.6 ± 8.9 (ID-MTs) for smooth muscle fibers ($t = 3.369$, $P = 0.028$).

IHC staining showed that the expression of α-SMA and smoothelin was much higher in the ID-MTs than in the NI-MTs after 7 days of implantation [Figure 7]. Semi-quantitative analysis demonstrated that the mean IOD

was 0.0613 ± 0.0172 (ID-MTs) *vs.* 0.002 ± 0.001 (NI-MTs) ($t = 5.994$, $P = 0.027$) for α-SMA and 0.0355 ± 0.0128 (ID-MTs) and 0.0035 ± 0.0022 (NI-MTs) ($t = 4.268$, $P = 0.013$) for smoothelin, thus suggesting that ID-MTs could maintain their phenotype in the bioprinted structure during the 7-day *in vivo* encapsulation process.

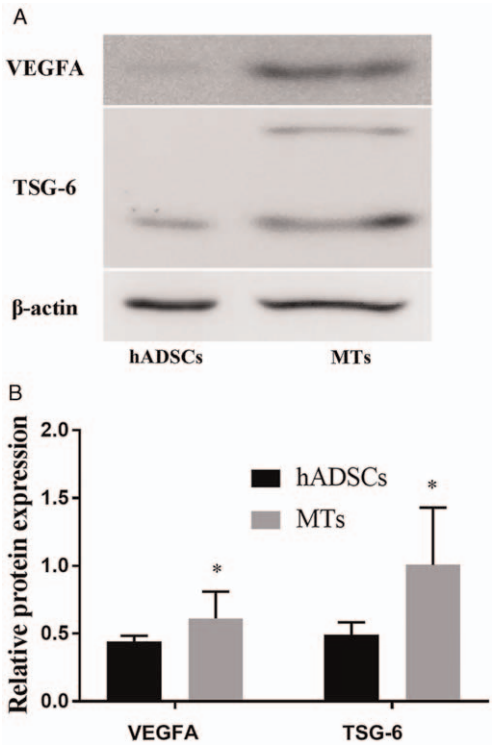

Figure 2: Detection of vascularization and anti-inflammation biomarkers in hADSCs and MTs. (A) Western blotting analysis comparing the relative protein expression of VEGFA and TSG-6 in a cultured monolayer of hADSCs and MTs. (B) Semi-quantitative data for relative protein expression (target protein/β-actin). *$P < 0.05$, comparison between the hADSCs and MTs. VEGFA: Vascular endothelial cell growth factor A; TSG-6: Tumor necrosis factor-alpha stimulated gene-6; hADSCs: Human adipose-derived stem cells; MTs: Microtissues.

Morphology and seeding of human ureteral urethelial cells onto encapsulated structures

After 7 to 10 days, primary culture of UCs was established, and passages 3 to 6 were employed for the next experiments. At passage 4, the UCs presented a typical cobblestone morphology [Figure 8A]. After seeding with UCs for 1 week, the UCs were viable and lined up mainly in a monolayer on the encapsulated structures, which incorporated ID-MTs/NI-MTs, as confirmed by immunofluorescent staining of AE1/AE3 [Figure 8B and 8C].

Discussion

Urinary tract reconstruction remains a challenging surgical intervention due to the shortage of appropriate biomaterials for replacement of urinary tract defects. Clinical autografting of tissue such as lingual or oral buccal mucosa and prepuce is often used for urethra reconstruction and yields satisfactory outcomes.[11-15] However, harvesting these autografts is traumatic and might cause complications including infection, bleeding, tricholithiasis, etc.[16] In addition, the limited source of these autografts restricts second chances at urinary tract reconstruction, which drives researchers to look for other substitutions. Under these circumstances, natural and synthetic biomaterials have been discovered for use in urinary tract reconstruction. Despite their advantages in biocapability and modifiability, both natural and synthetic biomaterials are unable to disperse cells into themselves. This means that cells are seeded onto the surface of these biomaterials and a wait is required to achieve infiltration,[2,3,17,18] thus

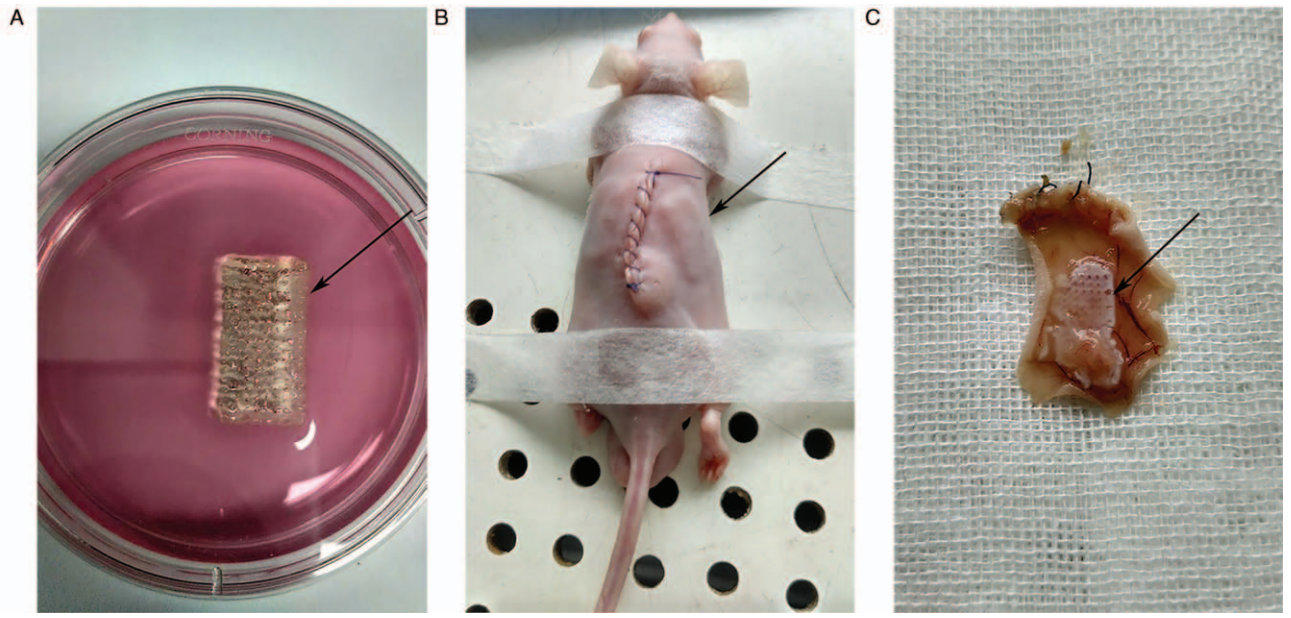

Figure 3: Morphology of freshly, implanted and retrieved 3D bioprinted structure. (A) Gross inspection of the freshly 3D bioprinted structure. (B) Subcutaneous implantation of the bioprinted structure into a nude mouse. (C) The retrieved structure after 1 week. The capsule of the bioprinted structure could be seen, as indicated by the black arrow. 3D: Three-dimensional.

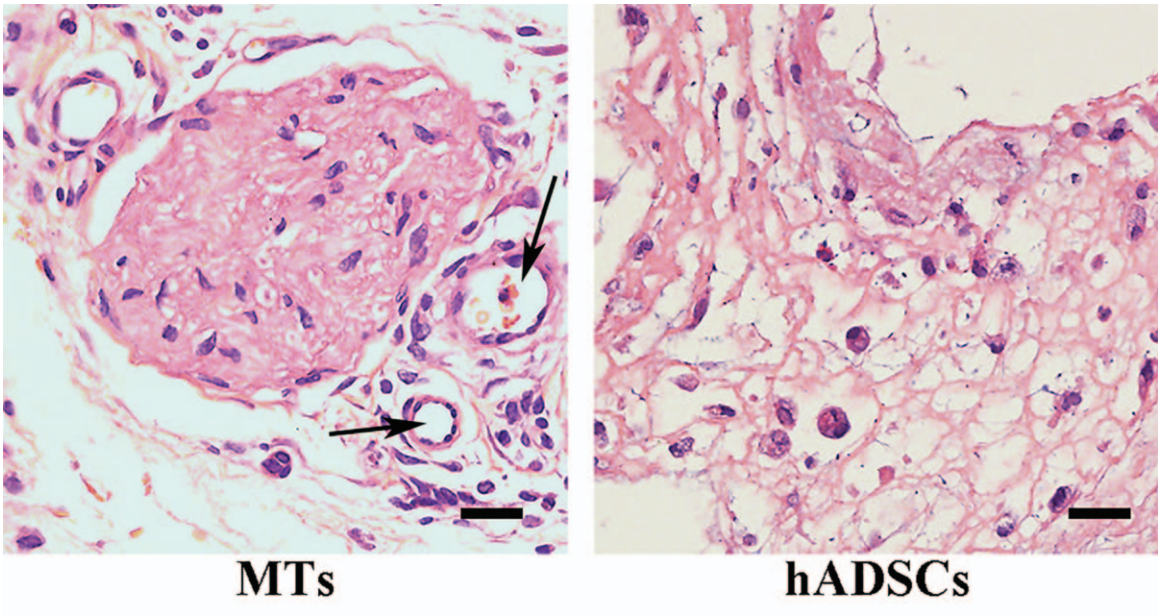

Figure 4: Hematoxylin and eosin staining of the retrieved structures. Left: MTs maintained their shape after bioprinting and the subcutaneous implantation process, and some vascular-like structure was observed around the MTs (indicated by the black arrow). Right: hADSCs in the retrieved structure had taken on a round shape, and vascular-like structures could hardly be observed. Scale bar = 20 μm. MTs: Microtissues; hADSCs: Human adipose-derived stem cells.

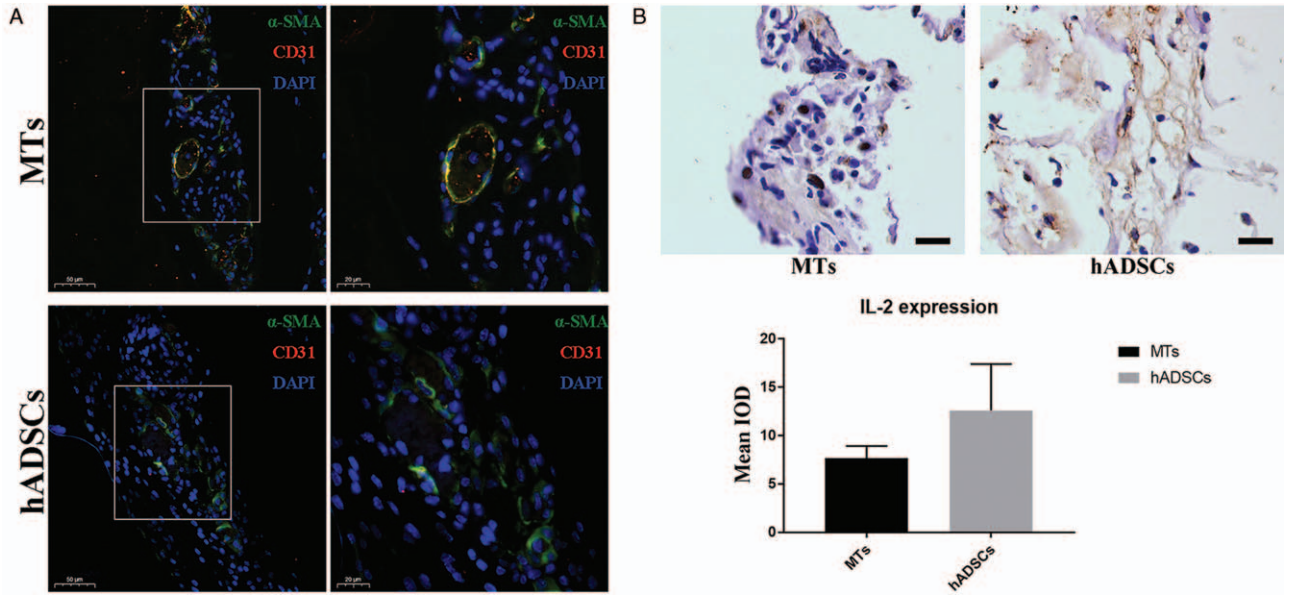

Figure 5: Immunofluorescent double staining of α-SMA and CD31 for the detection of neo-vascularization. (A) After 7 days of subcutaneous implantation, $CD31^+$ cells were observed localized in and around the α-SMA-positive vascular-like structure. Higher magnification of the boxed area in left panel further demonstrated the location of the $CD31^+$ cells (right). Scale bar = 50 and 20 μm. (B) Immunohistochemistry staining of IL-2 revealed that the retrieved structure constructed from MTs tended to express IL-2 at lower levels than their counterpart made from hADSCs (top). Semi-quantitative analysis indicated that there was no statistical significance in the difference of IL-2 expression between these two groups (bottom). Scale bar = 20 μm. α-SMA: α-Smooth muscle actin; IL-2: Interleukin-2; IOD: Integral optical density; MTs: Microtissues; hADSCs: Human adipose-derived stem cells.

prolonging their preparation time and limiting their further application.

The 3D bioprinting has shed light on tissue engineering. Compared to the traditional cell-infiltration strategy, 3D bioprinting can be used to fabricate a computer-designed construct of cells and bioinks, which accelerates the process of building a tissue-engineered structure and makes it possible to produce "off the shelf" substitutes for the replacement of defective native tissue. In the present study, we employed 3D bioprinting to fabricate smooth muscle-ID-MTs into a designed structure and encapsulated the bioprinted structures through subcutaneous implantation into nude mice. HE staining showed that after 1 week

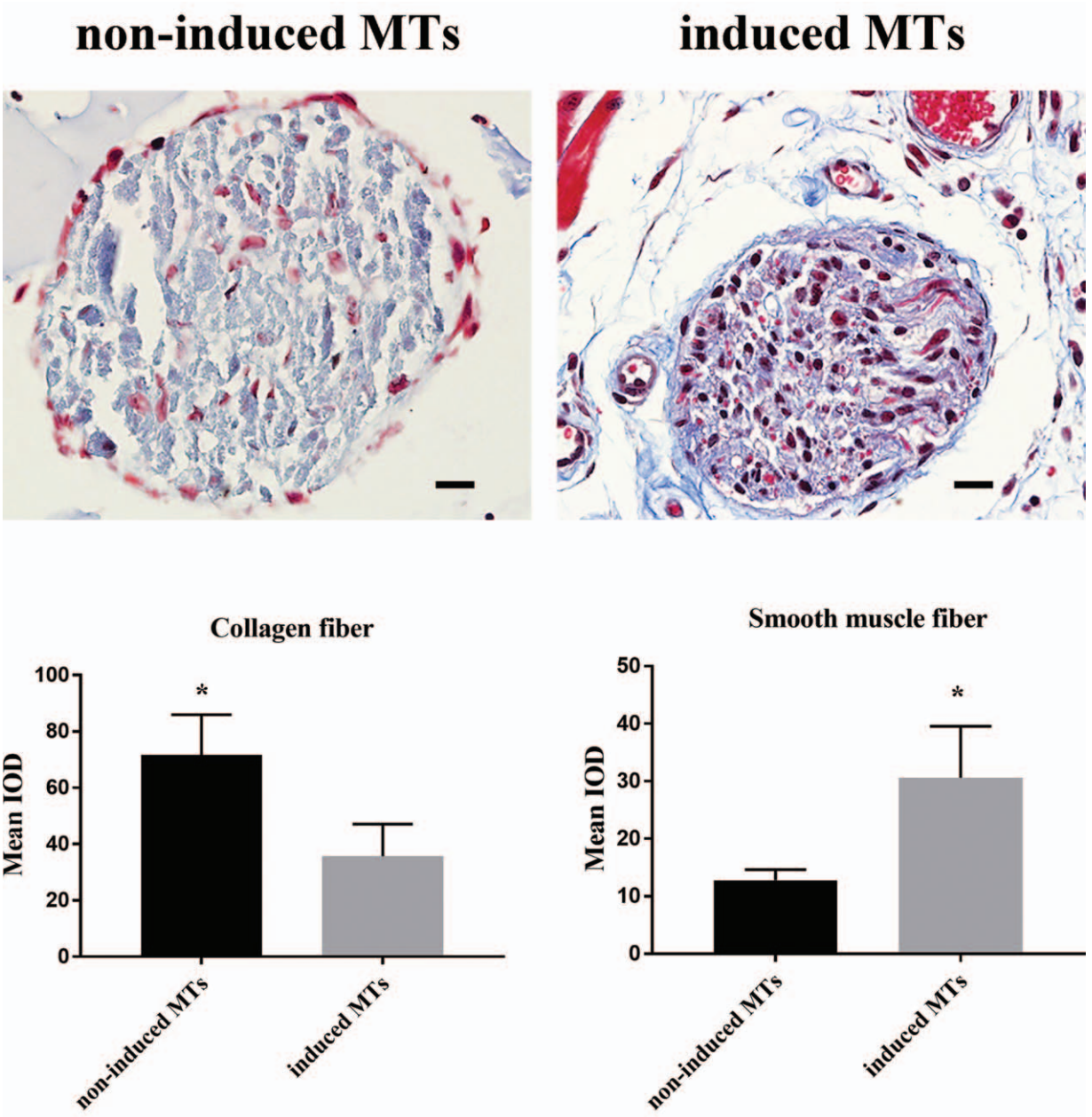

Figure 6: Masson's trichrome staining and semi-quantitative analysis for the revealing of collagen and smooth muscle fiber in MTs. Top: Masson's trichrome staining compared the formation of collagen fiber and smooth muscle fiber between the non-induced MTs group and the induced MT group. Bottom: Semi-quantitative analysis exhibited a statistical significance in the difference between these two groups. $*P < 0.05$, comparison between the non-induced MTs and induced MTs. Scale bar = 20 μm. IOD: Integral optical density; MTs: Microtissues.

of implantation, the MTs largely preserved their morphology, and Masson's trichrome staining revealed that NI-MTs were collagen fiber-rich and smooth muscle fiber depleted, while ID-MTs were the opposite, suggesting that the implanted structure utilizing ID-MTs could mimic the smooth muscle layer of native urinary tract.

One of the major concerns for tissue engineering is vascularization and anti-inflammation of the fabricated structure because grafts from natural or synthetic biomaterials for urinary tract reconstruction often end up failing due to lack of blood supply and the presence of inflammation or immunorejection. Although our previous investigation indicated that MTs gain better cell viability than single cells during the 3D bioprinting process,[9] vascularization, and anti-inflammation still play a crucial role in the survival of the implanted structure and the fate of the incorporated MTs. Many researchers have discovered various ways to enhance the vascularization of tissue-engineered structures. Heller *et al*[7] constructed tissue-engineered buccal mucosa by triculturing epithelial cells, endothelial cells, and fibroblasts in a native collagen membrane. The results verified that the capillary-like structures in the native membrane became functional blood vessels through anastomosis with host vasculature after implantation into nude mice. Wang *et al*[4] wrapped PLGA nanospheres with VEGF and modified a BAM graft with these nanospheres to reconstruct rabbit urethra. Their

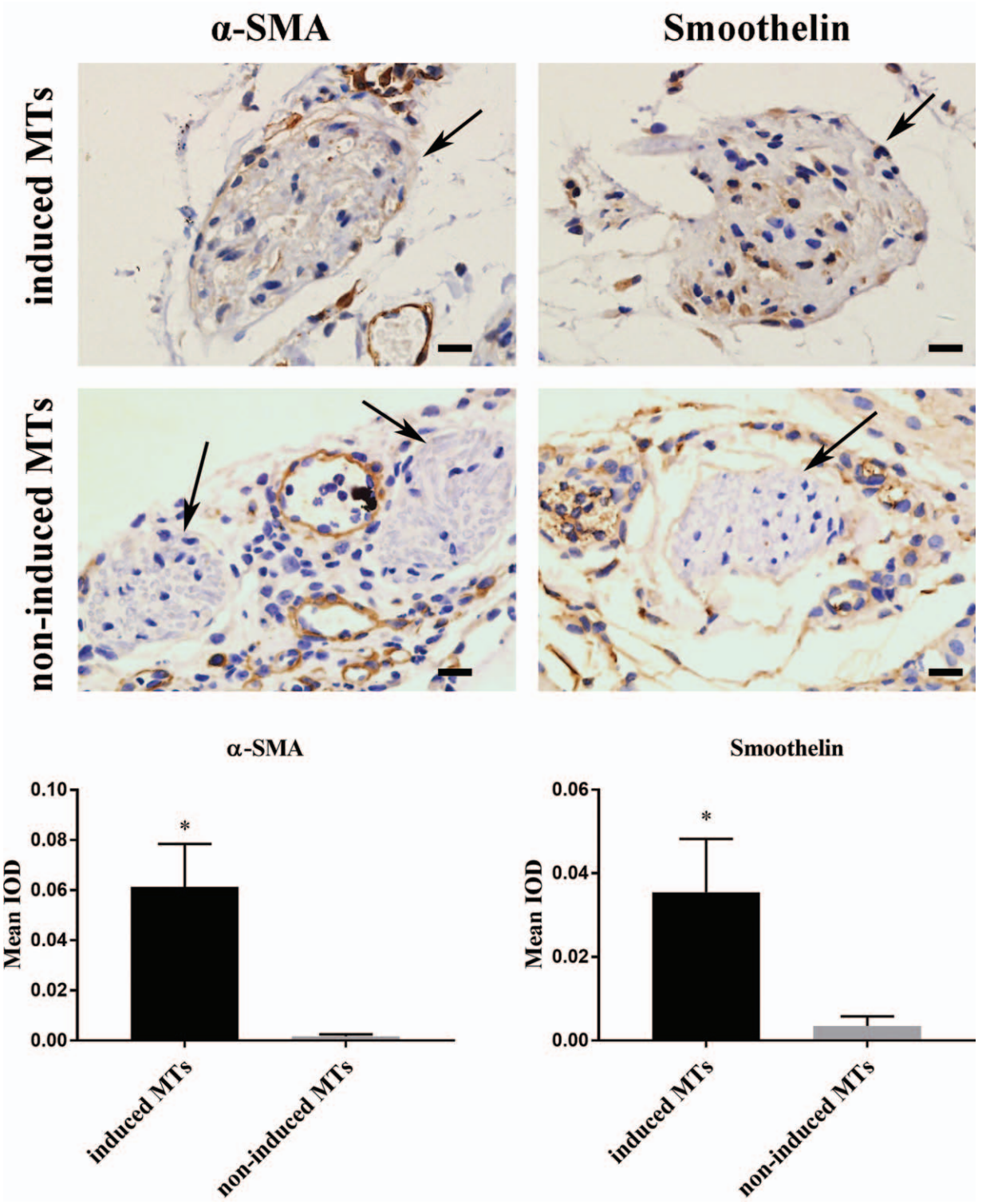

Figure 7: Immunohistochemistry and semi-quantitative analysis for the discovery of smooth muscle biomarkers in MTs. Top: Immunohistochemistry staining of α-SMA and smoothelin in non-induced and induced MTs. Bottom: Both α-SMA and smoothelin were expressed in induced MTs after 7 days of subcutaneous implantation, and non-induced MTs had little expression of these smooth muscle markers. Bottom: Semi-quantitative analysis indicated statistical significance in the difference in smooth muscle marker expression between induced and non-induced MTs. Scale bar = 20 μm. $^*P < 0.05$, comparison between induced MTs and non-induced MTs. IOD: Integral optical density; MTs: Microtissues; α-SMA: α-Smooth muscle actin.

results suggested that anterior urethra reconstruction with the sustained-release of VEGF by PLGA nanospheres-modified BAMG stents could reduce postoperative restenosis. Another interesting study conducted by Jia *et al*[19] showed that collagen scaffold bound with collagen-binding VEGF (VEGF) could promote urethral tissue regeneration and improve the function of the neo-urethra in an extensive urethral defect beagle model. In this research, the expression of VEGFA and TSG-6 was investigated with a Western blotting assay, and the results

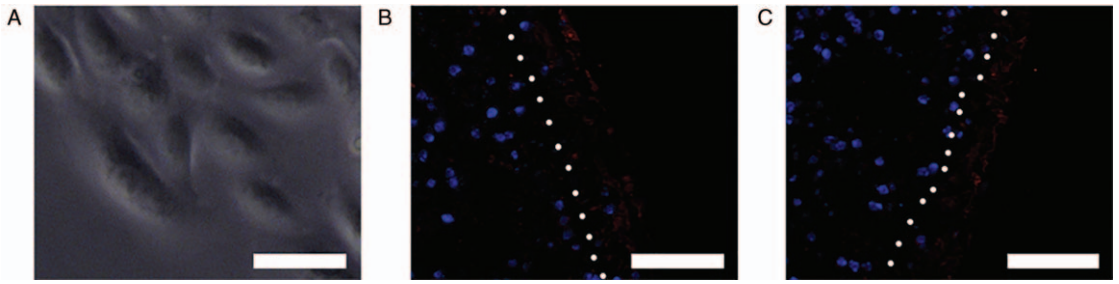

Figure 8: Morphology of urothelial cells and immunofluorescent staining of cytokeratins AE1/AE3 for encapsulated structures containing non-induced MTs/induced MTs seeded with urothelial cells. (A) Inverted microscopy demonstrated the cobblestone appearance of the human UCs in culture. (B) Immunofluorescent staining of UCs seeded onto encapsulated structures containing non-induced MTs were positive for cytokeratins AE1/AE3 (red). (C) Immunofluorescent staining of UCs seeded onto encapsulated structures containing non-induced MTs were positive for cytokeratins AE1/AE3 (red). After 1 week of seeding, UCs formed mainly a monolayer on the surface of the encapsulated structures (right of the white dotted line). Scale bar = 50 μm. MTs: Microtissues; UCs: Urothelial cells.

demonstrated that both VEGFA and TSG-6 were expressed at a much higher level in MTs than in monolayer-cultured hADSCs, which is consistent with our previous study.[10] A similar investigation was performed by Freeman *et al*[20] They pre-vascularized chondrogenically primed human mesenchymal stem cell (MSCs) aggregates by culturing them in endothelial growth medium, and then the aggregates were implanted into nude rats. The results showed that the pre-vascularized cartilaginous aggregates formed mature endogenous vessels. In comparison with the aforementioned studies, our present study revealed that MTs of hADSCs could express VEGFA without any other manipulation and, thus, shed light on vascularization *in vivo* when MTs were employed for tissue-engineered structures instead of the classic single-cell strategy. Moreover, immunofluorescent staining of CD31 and α-SMA in the retrieved structure confirmed neo-vascularization in the MTs group, while the monolayer hADSC group only had little neo-vascularization. For anti-inflammation, TSG-6 is a well-known anti-inflammatory protein that has been investigated by many scholars. Among these studies, Magaña-Guerrero *et al*[21] found that conditioned medium from human amniotic mesenchymal stem cells was able to diminish the release of neutrophil extracellular traps (NETs), and TSG-6 participates in the inhibition mechanism of reactive oxygen species-dependent NETs. Yun *et al*[22] identified that both mesenchymal stromal cells derived from induced pluripotent stem cells (MSCs) and bone marrow-derived MSCs exert therapeutic effects in the cornea by reducing inflammation in part through the expression of TSG-6. Previous research conducted by Zhou *et al*[23] utilized MTs constructed of hADSCs to treat erectile dysfunction in streptozotocin-induced diabetic rats, and the results verified that the MTs expressed VEGF, nerve growth factor, and TSG-6, which was partly similar to our present study. Attractively, we noticed that even in monolayer-cultured hADSCs, there was also expression of TSG-6 to some degree, suggesting that hADSCs have the potential to alleviate inflammation, in accordance with the results of Song *et al*.[24] Nevertheless, the higher expression of TSG-6 in MTs makes them a preferable candidate for fabricating tissue-engineered structures. In the following IHC results, the observed trend that the expression of IL-2 was lower in MTs than in hADSCs confirmed that bioprinted structures containing MTs might cause milder immunorejection, since IL-2 is a useful indicator of this type of inflammation.[25,26]

In our previous study, we found that combining hanging-drop cultures with SMIM could enhance the smooth muscle differentiation of hADSCs *in vitro*,[9] but whether or not ID-MTs could maintain their phenotype *in vivo* was still unknown. According to studies conducted by other researchers, when cells infiltrate the biomaterials, their phenotypes might be changed and impose a negative effect on cell function.[27] Therefore, IHC was employed to examine the phenotype of ID-MTs in the bioprinted structure after subcutaneous implantation, and NI-MTs were set as the control. After 7 days of implantation, the expression of α-SMA and smoothelin in ID-MTs indicated the stability of their phenotypes, while NI-MTs had little expression of these two smooth muscle markers. These results supported the use of MTs to create a supporting matrix, or so-called substrate, for UCs by bioprinting a urinary tract patch.

Urothelial tissue plays an important role in native urinary tract due to its barrier function, which prevents urine leakage into deeper tissue layers.[28] In our previous study, the subcutaneous implantation of a poly (L-lactic acid) scaffold into nude mice could induce the formation of capsules on the structure,[29] and it was proven that the entrapped UCs lined up mainly in a monolayer on the capsular stents within an embedding period of 1 week. In the present study, we isolated and expanded human UCs from the ureter and then seeded the UCs onto the encapsulated structure. The results of immunofluorescence showed the expression of urothelial marker AE1/AE3 on the encapsulated structure, revealing that the UCs formed monolayer on the bioprinted urinary tract patch, thus developing a "barrier" to protect the bioprinted urinary tract patch from urine seepage.

In conclusion, we built a tissue-engineered urinary tract patch by combining 3D bioprinting and subcutaneous implantation. The results from Western blotting and histology analysis demonstrated that the ID-MTs consisting of hADSCs might be a preferable candidate for use in constructing a urinary tract patch for UC adhesion. Further investigation is required to examine its effectiveness for urinary tract reconstruction in an animal model.

Funding

This work was supported by a grant from the National Natural Science Foundation of China (No. 81570601).

Conflicts of interest

None.

References

1. Liu Y, Ma W, Liu B, Wang Y, Chu J, Xiong G, *et al*. Urethral reconstruction with autologous urine-derived stem cells seeded in three-dimensional porous small intestinal submucosa in a rabbit model. Stem Cell Res Ther 2017;8:63. doi: 10.1186/s13287-017-0500-y.
2. Li H, Xu Y, Xie H, Li C, Song L, Feng C, *et al*. Epithelial-differentiated adipose-derived stem cells seeded bladder acellular matrix grafts for urethral reconstruction: an animal model. Tissue Eng Part A 2014;20:774–784. doi: 10.1089/ten.TEA.2013.0122.
3. Wang Y, Fu Q, Zhao RY, Deng CL. Muscular tubes of urethra engineered from adipose-derived stem cells and polyglycolic acid mesh in a bioreactor. Biotechnol Lett 2014;36:1909–1916. doi: 10.1007/s10529-014-1554-x.
4. Wang JH, Xu YM, Fu Q, Song LJ, Li C, Zhang Q, *et al*. Continued sustained release of VEGF by PLGA nanospheres modified BAMG stent for the anterior urethral reconstruction of rabbit. Asian Pac J Trop Med 2013;6:481–484. doi: 10.1016/s1995-7645 60078-4.
5. Feng C, Xu YM, Fu Q, Zhu WD, Cui L. Reconstruction of three-dimensional neourethra using lingual keratinocytes and corporal smooth muscle cells seeded acellular corporal spongiosum. Tissue Eng Part A 2011;17:3011–3019. doi: 10.1089/ten.TEA.2011.0061.
6. Arenas da Silva LF, Micol L, Tiemessen D, van Kuppevelt TH, Frey P, Oosterwijk E, *et al*. Is there a need for smooth muscle cell transplantation in urethral reconstruction? Tissue Eng Part A 2014;20:1542–1549. doi: 10.1089/ten.TEA.2013.0185.
7. Heller M, Frerick-Ochs EV, Bauer HK, Schiegnitz E, Flesch D, Brieger J, *et al*. Tissue engineered pre-vascularized buccal mucosa equivalents utilizing a primary triculture of epithelial cells, endothelial cells and fibroblasts. Biomaterials 2016;77:207–215. doi: 10.1016/j.biomaterials.2015.10.073.
8. Liu Y, Bharadwaj S, Lee SJ, Atala A, Zhang Y. Optimization of a natural collagen scaffold to aid cell-matrix penetration for urologic tissue engineering. Biomaterials 2009;30:3865–3873. doi: 10.1016/j.biomaterials.2009.04.008.
9. Yipeng J, Yongde X, Yuanyi W, Jilei S, Jiaxiang G, Jiangping G, *et al*. Microtissues enhance smooth muscle differentiation and cell viability of hADSCs for three dimensional bioprinting. Front Physiol 2017;8:534. doi: 10.3389/fphys.2017.00534.
10. Xu Y, Guan R, Lei H, Li H, Wang L, Gao Z, *et al*. Therapeutic potential of adipose-derived stem cells-based micro-tissues in a rat model of postprostatectomy erectile dysfunction. J Sex Med 2014;11:2439–2448. doi: 10.1111/jsm.12636.
11. Vasudeva P, Nanda B, Kumar A, Kumar N, Singh H, Kumar R. Dorsal versus ventral onlay buccal mucosal graft urethroplasty for long-segment bulbar urethral stricture: a prospective randomized study. Int J Urol 2015;22:967–971. doi: 10.1111/iju.12859.
12. Liu Y, Zhuang L, Ye W, Ping P, Wu M. One-stage dorsal inlay oral mucosa graft urethroplasty for anterior urethral stricture. BMC Urol 2014;14:35. doi: 10.1186/1471-2490-14-35.
13. Soliman MG, Abo Farha M, El Abd AS, Abdel Hameed H, El Gamal S. Dorsal onlay urethroplasty using buccal mucosa graft versus penile skin flap for management of long anterior urethral strictures: a prospective randomized study. Scand J Urol 2014;48:466–473. doi: 10.3109/21681805.2014.888474.
14. Sharma AK, Chandrashekar R, Keshavamurthy R, Nelvigi GG, Kamath AJ, Sharma S, *et al*. Lingual versus buccal mucosa graft urethroplasty for anterior urethral stricture: a prospective comparative analysis. Int J Urol 2013;20:1199–1203. doi: 10.1111/iju.12158.
15. Zhang K, Zhou S, Zhang Y, Xu Y, Jin S, Sa Y, *et al*. Anterior urethra reconstruction with lateral lingual mucosa harvesting technique. Urology 2016;90:208–212. doi: 10.1016/j.urology.2016.01.008.
16. Atala A, Danilevskiy M, Lyundup A, Glybochko P, Butnaru D, Vinarov A, *et al*. The potential role of tissue-engineered urethral substitution: clinical and preclinical studies. J Tissue Eng Regen Med 2017;11:3–19. doi: 10.1002/term.2112.
17. Lv XG, Feng C, Fu Q, Xie H, Wang Y, Huang JW, *et al*. Comparative study of different seeding methods based on a multilayer SIS scaffold: which is the optimal procedure for urethral tissue engineering? J Biomed Mater Res B Appl Biomater 2016;104:1098–1108. doi: 10.1002/jbm.b.33460.
18. Dinescu S, Galateanu B, Albu M, Cimpean A, Dinischiotu A, Costache M. Sericin enhances the bioperformance of collagen-based matrices preseeded with human-adipose derived stem cells (hADSCs). Int J Mol Sci 2013;14:1870–1889. doi: 10.3390/ijms14011870.
19. Jia W, Tang H, Wu J, Hou X, Chen B, Chen W, *et al*. Urethral tissue regeneration using collagen scaffold modified with collagen binding VEGF in a beagle model. Biomaterials 2015;69:45–55. doi: 10.1016/j.biomaterials.2015.08.009.
20. Freeman FE, Allen AB, Stevens HY, Guldberg RE, McNamara LM. Effects of in vitro endochondral priming and pre-vascularisation of human MSC cellular aggregates in vivo. Stem Cell Res Ther 2015;6:218. doi: 10.1186/s13287-015-0210-2.
21. Magaña-Guerrero FS, Domínguez-López A, Martínez-Aboytes P, Buentello-Volante B, Garfias Y. Human amniotic membrane mesenchymal stem cells inhibit neutrophil extracellular traps through TSG-6. Sci Rep 2017;7:12426. doi: 10.1038/s41598-017-10962-2.
22. Yun YI, Park SY, Lee HJ, Ko JH, Kim MK, Wee WR, *et al*. Comparison of the anti-inflammatory effects of induced pluripotent stem cell-derived and bone marrow-derived mesenchymal stromal cells in a murine model of corneal injury. Cytotherapy 2017;19:28–35. doi: 10.1016/j.jcyt.2016.10.007.
23. Zhou F, Hui Y, Xin H, Xu YD, Lei HE, Yang BC, *et al*. Therapeutic effects of adipose-derived stem cells-based microtissues on erectile dysfunction in streptozotocin-induced diabetic rats. Asian J Androl 2017;19:91–97. doi: 10.4103/1008-682x.182817.
24. Song WJ, Li Q, Ryu MO, Ahn JO, Ha Bhang D, Chan Jung Y, *et al*. TSG-6 secreted by human adipose tissue-derived mesenchymal stem cells ameliorates DSS-induced colitis by inducing M2 macrophage polarization in mice. Sci Rep 2017;7:5187. doi: 10.1038/s41598-017-04766-7.
25. Lun A, Cho MY, Muller C, Staffa G, Bechstein WO, Radke C, *et al*. Diagnostic value of peripheral blood T-cell activation and soluble IL-2 receptor for acute rejection in liver transplantation. Clin Chim Acta 2002;320:69–78. doi: 10.1016/s0009-8981(02)00045-1.
26. Xie H, Yang F, Deng L, Luo J, Qin T, Li X, *et al*. The performance of a bone-derived scaffold material in the repair of critical bone defects in a rhesus monkey model. Biomaterials 2007;28:3314–3324. doi: 10.1016/j.biomaterials.2007.04.001.
27. Lynn AD, Bryant SJ. Phenotypic changes in bone marrow-derived murine macrophages cultured on PEG-based hydrogels activated or not by lipopolysaccharide. Acta Biomater 2011;7:123–132. doi: 10.1016/j.actbio.2010.07.033.
28. Atala A. Experimental and clinical experience with tissue engineering techniques for urethral reconstruction. Urol Clin North Am 2002;29:485–492. doi: 10.1016/s0094-0143(02)00033-2.
29. Xu Y, Fu W, Li G, Shi J, Tan H, Hu K, *et al*. Autologous urothelial cells transplantation onto a prefabricated capsular stent for tissue engineered ureteral reconstruction. J Mater Sci Mater Med 2012;23:1119–1128. doi: 10.1007/s10856-012-4583-9.

How to cite this article: Jin YP, Shi C, Wu YY, Sun JL, Gao JP, Yang Y. Encapsulated three-dimensional bioprinted structure seeded with urothelial cells: a new construction technique for tissue-engineered urinary tract patch. Chin Med J 2020;133:424–434. doi: 10.1097/CM9.0000000000000654